Progress In Electromagnetics Research M, Vol. 50, 183–193, 2016

Analysis of the Static and Dynamic Behavior of a Non Hysteretic Superconductive Passive Magnetic Linear Bearing by Using an Electromagnetic Integral Formulation

Efren Diez-Jimenez[1], Antonino Musolino[2], Rocco Rizzo[2, *], and Ernesto Tripodi[2]

Abstract—In this paper the analysis of the static and dynamic behavior of a non-hysteretic superconductive passive linear bearing is described. The high translational symmetry of the magnetic field seen by the permanent magnet assures a usable long stroke in the order of several tens of millimeters. The linear bearing in combination with an actuating system for only one degree of freedom can be used for accurate long-stroke precision positioning systems for cryogenic environments with zero hysteresis in the movement. The dynamics of the system is investigated using an integral formulation which transforms the solution of the field equations in the solution of an equivalent electric network. The knowledge of the currents in the equivalent network allows to evaluate all the electromagnetic quantities (fields, forces, eddy currents, ...) in the system. Finally, the coupling with the equation of the rigid body permits to simulate the electro/mechanical behavior of the system with six degree of freedom (6 DOF).

1. INTRODUCTION

In many high-tech areas (aerospace industry, biomedical laboratories, optical communication, and so forth), the demand for very precise actuators, capable to operate in low temperature environment ($T < 100\,\mathrm{K}$), is increasing due to their specific features [1–3]. In this field, in fact, conventional mechanisms [4–6], which use bearings and joints, cannot be used, since lubrication fluids freeze at very low temperatures. Also solid lubricants such as PFTE or MoS2, usually used in cryogenic environment to mitigate the tribological problems, are not a very reliable solution due to a limited life-time operation [7, 8]. Devices based on active magnetic bearings can be used only in special cases [9, 10]. Since they exploit electrical coils to produce magnetic force, the activation currents can cause thermal problems in these temperature-sensitive environments.

The superconducting magnetic levitation (SML) seems to be a very suitable technology for the development of devices capable to assure accurate long-stroke precision positioning in cryogenic environments. SML assures the self-stable levitation of hard magnetic materials over a high temperature superconductor (HTS) [11, 12]. Although at cryogenic temperatures HTS are naturally in the superconducting state, two different behaviors should be considered. If the superconductor is not in the Meissner but in the mixed state, the hard magnetic materials levitates above the HTS but the levitating force-distance relationship is hysteretic [13], so depending on the applied field history. On the contrary, if the superconductor is in the Meissner state, the levitation force vs distance is a non-hysteretic relation, allowing to increase the stability region and the performance of the SML-based devices [14]. Anyhow, the technological challenges to design stable levitating system while keeping the HTS in the Meissner state are an open issue.

Received 23 June 2016, Accepted 3 September 2016, Scheduled 5 October 2016

* Corresponding author: Rocco Rizzo (rocco.rizzo@unipi.it).

[1] Mechanical Engineering Area, Universidad de Alcalá, Spain. [2] Department of Energy and Systems Engineering, University of Pisa, Italy.

Some mechanisms based on superconducting magnetic levitation were developed in the past, with potential uses such as in precision positioning or magnetic confinement. Unfortunately, the main drawback of these solutions is the length of the strokes when being applied to precise non-contact actuators. For example, in [15] the stroke length was limited to a few millimeters ($< 10\,\text{mm}$) with a resolution in the range of μm, while in [16, 17] the authors described a SML-based linear bearing, claiming a maximum stroke of 18 mm in one direction with very high resolution.

In a previous paper [18], the authors presented the mechanical design of a magnetic levitating linear bearing, suitable for working in the non-hysteretic range of forces, also assuring a usable long stroke of around $\pm 90\,\text{mm}$ with full performance and $\pm 150\,\text{mm}$ with reduced performance. In the same paper, the analysis of forces and pressures for each direction was performed by using a finite element model. The results demonstrated that the SML-based device provided stable equilibrium positioning and restoring forces in all degrees of freedom (DOF) except for two (rotation and displacement along the axis of motion) with a cylindrical magnet floating along the axis of revolution/displacement. The linear bearing was investigated under static conditions, and the radial and axial stiffness of the bearing was calculated.

From a numerical point of view, the coupled electromechanical analysis necessary to assess the dynamical behavior of a 6 DOF system is a challenging task. Although the finite-element method (FEM) is the most popular approach to simulate complex electromagnetic systems, it may suffer some limitations especially when dealing with bodies in movement. The application of FEM to systems with moving conductors presents some difficulties, mainly due to the coupling of meshes attached to bodies in relative motion in all the spatial directions [19]. They usually require a large number of unknowns to obtain a desired accuracy [20]. Furthermore, the meshes and consequently the matrices involved in the calculations have to be updated during the motion and the analysis of unbounded domains requires special treatments [21]. Alternative approaches, mostly based on integral formulations such as the one used in this paper, have a number of characteristics that make them well suited for the analysis of electromechanical systems [22]. In particular, the problem of coupling moving meshes does not arise when integral formulation is used to simulate these kind of systems, since only the discretization of the active regions is required. However, the integral formulations also present some limitations, usually related to the numerical solution of the model. In fact, the main drawback is the matrix setup time and matrix solution time. A device discretized in n elementary volumes requires the evaluation of n^2 multidimensional integrals of Green functions that are arranged in densely populated matrices. Fortunately, integral formulations are inherently parallelizable [23], and the use of multicore CPUs or GPUs can reduce computation times.

In the present work, the analysis of the statics and dynamics behavior of a non hysteretic superconductive passive magnetic linear bearing is presented. With respect to the analysis described in [18], the innovation point consists in the use of a different formulation capable to simulate also the dynamic behavior of the superconductive device. In fact, in [18] only static FEM simulations of the device with a reduced number of DOF were described. Unfortunately, in that paper the analysis of the device cannot be satisfactorily extended to simulate the full 6 DOF dynamic behavior, due to the above cited limitations of the FE model.

In this manuscript, instead, the investigation is performed by the use of an electromagnetic numerical code based on a 3D integral formulation and capable to overcome the limitations of the FEM model. This code (hereafter referred to as "Equivalent Network for Electromagnetic Modeling — EN4EM" was developed in the past years at the University of Pisa for research purposes [24–26], and it is here adapted to deal with SML-based devices, dynamically operating with 6 DOF.

2. BRIEF DESCRIPTION OF THE DEVICE CHARACTERISTICS

Refer to the cited paper ([18]) for a detailed description of this SML-based linear bearing and its operation. For the sake of subsequent clarity, here below the main characteristics are described.

As shown in Fig. 1, the levitating device consists of a U-shaped superconducting (SC) surface and a magnetic cylinder with magnetization orientation perpendicular to the U-shaped plane, which is parallel to the x-axis. The superconducting material has been smoothed in the lateral sides in order to assure that a cylindrical magnet can float along the x-axis, and can be into a stable equilibrium in the remaining

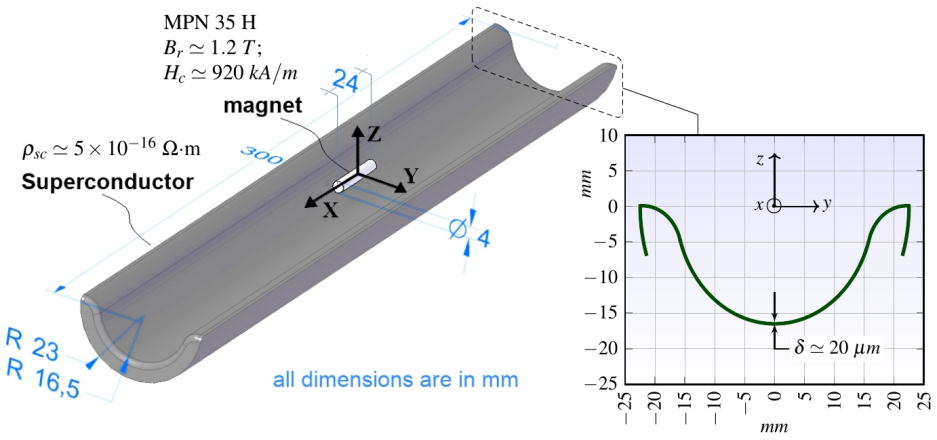

Figure 1. Geometrical definition and reference frame.

degrees of freedom (DOF), due to restoring forces. This solution is very suitable for long-stroke precision positioning systems for cryogenic environments with zero hysteresis in the movement. Furthermore, the length of the motion range can be easily modified by simply increasing the superconducting guideway.

The numerical analysis was carried out considering the superconductor as a conductive material with very low electrical resistivity ($5 \times 10^{-16}\ \Omega$·m) and really small depth ($\delta \simeq 20 \times 10^{-6}$ m). The profile of the SC surface and the reference frame used in the numerical model are shown in Fig. 1.

The NdFeB permanent magnet (grade MPN 35H) has a remanence $B_r = 1.21$ T and a coercivity $H_c = -920$ kA/m. Assuming that the magnetization vector $\mathbf{M}$ is uniform inside the material, the magnet can be simulated as a conducting sheet (see Fig. 2) with a thickness of the same order of magnitude of the superconductor surface depth. As for the relative permeability of the magnet, although the accurate value is about $\mu_r = B_r/|H_c|/\mu_0 = 1.047$, in order to simplify the numerical model it is approximated to the unity. The equivalent magnetization current on the sheet has been calculated as a bound surface current density starting from: $\mathbf{J}_{sb}(\mathbf{r}') = \mathbf{M}(\mathbf{r}') \times \mathbf{a}'_s$, where $\mathbf{a}'_s$ is a unit vector pointing out of the closed surface of the magnet.

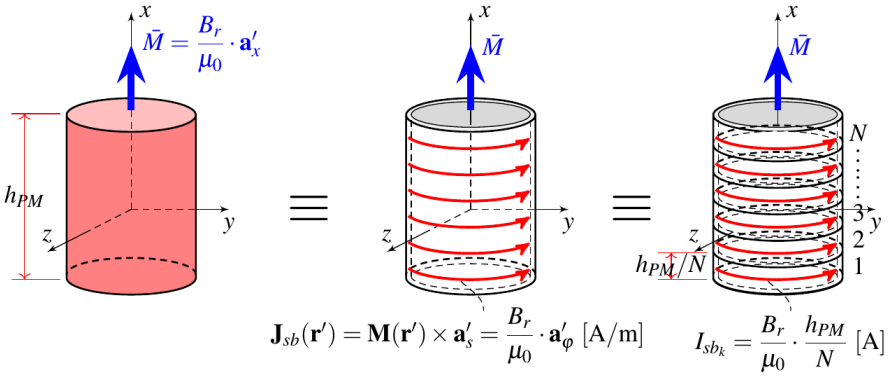

Figure 2. Permanent magnet model.

The total equivalent current flowing on the cylinder lateral surface is:

$$I_{sb} = \frac{B_r}{\mu_0} \cdot h_{PM} \tag{1}$$

where h_{PM} is the height of the cylinder magnet. Then, in order to avoid numerical inaccuracies, the magnet has been modeled with a stack of circular loops each carrying a fraction of the total current:

$$I_{sb_k} = \frac{B_r}{\mu_0} \cdot \frac{h_{PM}}{N}, \text{ with } k = 1, 2, \ldots, N. \tag{2}$$

In a real SML-based system, the current density inside the superconducting material is generated by the motion of the PM cylinder from infinity (that is, from a point far enough to not excite the SC) to a point in the vicinity of the U-shaped SC (i.e., the center of the reference frame). In the numerical model, this physical transient phase can be simulated by placing the magnet in the center of the reference frame and assuming that the equivalent magnetization current which model the PM varies as a transient function of time t, described by the following equation and shown in Fig. 3.

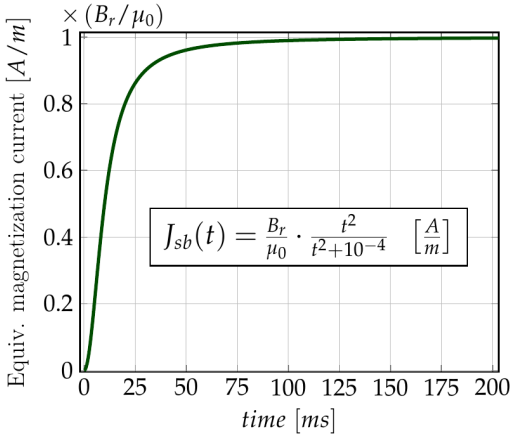

Figure 3. Equivalent magnetization current transient.

3. THE NUMERICAL CODE: SYNTHESIS

The numerical code used to simulate the system is based on a 3D integral formulation; it can simulate complex electromagnetic devices, transforming the solution of the field equations in the solution of an equivalent electric network [24, 28]. In fact, the code allows to obtain a set of equations that can be seen as the equilibrium equations set of an equivalent electric network. The currents in the branches of such auxiliary network correlate with the currents in elementary volumes in which the devices are discretized. Then, the knowledge of these currents allows to evaluate all the electromagnetic quantities (fields, forces, eddy currents, ...) in the real devices. Coupling with the equation of the rigid body (6 DOF) is performed by the terms: $\mathbf{v}_k \times \mathbf{B}_k$ and $\mathbf{J}_k \times \mathbf{B}_k$.

The main numerical formulation characteristics are: (a) only active (usually conductive) parts of a device must be discretized; (b) coupling with external lumped circuits is straightforward. The main drawbacks, instead, are the matrix setup time and the matrix solution time. These matrices are densely populated, and this may require (relatively) long computational times to get the solution. Anyhow, since this formulation is highly parallelizable, recent improvements in multicore CPUs or GPUs, allows to reduce the computation time [23, 26].

Consider two bodies in relative motion, with or without contact, and magnetically interacting (see Fig. 4); they can be discretized with n and m elementary volumes. Then, connecting the centers of nearby elements a 3-D grid can be obtained.

Assuming that inside each elementary volume the current densities (sources, induced, magnetization) are uniform and have only one non-zero component, the Ohm's Law is:

$$\rho \mathbf{J}_k = \mathbf{E}_k = -\nabla V_k - \frac{\partial \mathbf{A}_k}{\partial t} + \mathbf{v}_k \times \mathbf{B}_k; \tag{3}$$

then, by using the additive property, it can be written as:

$$-\nabla V_k = \rho \mathbf{J}_k + \sum_{j=1}^{N} \frac{\partial \mathbf{A}_{k,j}}{\partial t} - \mathbf{v}_k \times \sum_{j=1}^{N} \mathbf{B}_{k,j}; \tag{4}$$

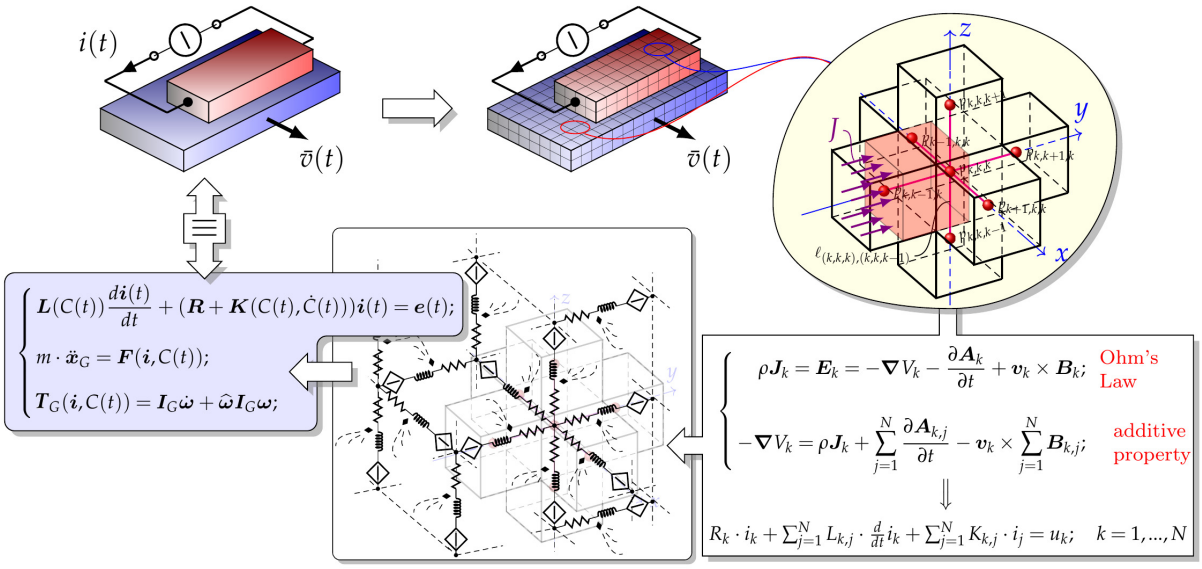

Figure 4. Scheme of the numerical code used for the simulations.

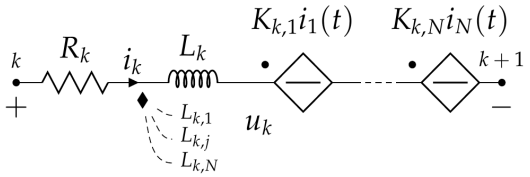

Figure 5. Equivalent electric branch.

where $N = n + m$ is the number of elementary volumes, and the other quantities are the well-known electromagnetic vectors/scalars.

Integrating the Ohm's law in each elementary volume and averaging the result on the cross section it is possible to obtain an equation which represents the electric equilibrium equation of a branch of a network. As shown in Fig. 5, this branch can be drawn as a series connection of a resistor, an inductor coupled with the inductors in other branches and controlled voltage generators that take into account the motional effects. Then, it can be described by using the Kirchhoff's voltage law.

Extending the procedure to the whole system it is possible to obtain a complete equivalent electric network, which can be studied by the mesh analysis, yielding to a set of electrical equations.

Once the currents are known, the force $\mathbf{f}_{kj}$ exerted on the kth elementary volume due to the jth one can be calculated as follows [27]. In correspondence to a given configuration, the dynamic interactions between couples of elementary volumes (one on the fixed body and one on the moving one) were firstly evaluated in the hypothesis of unit current on them. In this way, it is possible to obtain the force coefficients $\mathbf{\Lambda}_{kj}$ which are function of the geometric configuration of the system. Subsequently the effective force on the elementary volumes which constitute the moving body can be calculated as:

$$\mathbf{f}_{kj} = \int_{\Gamma_k} \mathbf{J}_k \times \mathbf{B}_j d\Gamma = \mathbf{\Lambda}_{kj} \mathbf{i}_k \mathbf{i}_j \tag{5}$$

where k and j span respectively the elementary volumes of the moving body and of the fixed one, while $\mathbf{i}_k$ and $\mathbf{i}_j$ are the effective currents flowing on them.

By summing the effects of all this terms, the resultant force on the k-th elementary volume of the

moving body can be calculated:

$$\mathbf{F}_k = \sum_{j=1}^{N_f} \mathbf{f}_{kj} \quad k = N_f + 1, \ldots, N_f + N_m \tag{6}$$

The set of $\mathbf{F}_k$ represents the force distribution on the rigid body. Finally, summing up the contributions to all the elementary volumes of the moving body, we obtain the resultant force and torque, and consequently the complete set of coupled equations:

$$\begin{cases} \mathbf{L}(\mathbf{C}(t))\frac{d\mathbf{i}(t)}{dt} + \left[\mathbf{R}(\mathbf{C}(t)) + \mathbf{K}(\mathbf{C}(t), \dot{\mathbf{C}}(t))\right] \mathbf{i}(t) = \mathbf{e}(t); \\ m \cdot \ddot{\mathbf{x}}_G = \mathbf{F}(\mathbf{i}, \mathbf{C}(t)); \\ \mathbf{T}_G(\mathbf{i}, \mathbf{C}(t)) = \mathbb{I}_G \dot{\boldsymbol{\omega}} + \widehat{\boldsymbol{\omega}} \mathbb{I}_G \boldsymbol{\omega}; \end{cases} \tag{7}$$

where: $\mathbf{C}(t)$ is the system configuration matrix (a function of the coordinates and Euler angles of the center of gravity of all the elementary volumes), $\mathbf{i}(t)$ the vector of the currents in the elementary volumes and $\mathbf{e}(t)$ the vector of the applied voltage generators. It is worth to note that $\mathbf{i}(t)$ include the equivalent magnetization currents and that some of the currents may be imposed.

$\mathbf{L}(\mathbf{C}(t))$ denotes the inductance matrix, $\mathbf{R}(\mathbf{C}(t))$ is the resistance matrix, and $\mathbf{K}(\mathbf{C}(t), \dot{\mathbf{C}}(t))$ considers the electromotive force due to the motional effects. In particular $\dot{\mathbf{C}}(t)$, termed as the derivatives of the system configuration at the instant t, describes the velocity of every elementary volume. $\mathbf{F}$ and $\mathbf{T}$ are, respectively, the resultant force and torque acting on the moving body, m is its mass, and $\mathbb{I}_G$ is the inertia tensor. The three components vectors $\ddot{\mathbf{x}}_G$ and $\boldsymbol{\omega}$, respectively, indicate the coordinates of the center of mass of the moving body and its angular velocity. It is worth to note that $\mathbf{F}$ and $\mathbf{T}$ are functions of $\mathbf{C}(t)$ and of the currents on the elementary volumes.

Since the differential equations for the electrical and dynamic equilibrium are coupled, the resulting system is nonlinear and time varying. However, the electrical equations are integrated by using a conventional integration scheme (Single Step Time Marching) [27]. The solution of the model allows to know all the electromagnetic and mechanical quantities which govern the operation of a given 6 DOF device.

Figure 6 shows the mesh used by the numerical code to simulate the superconductive passive magnetic linear bearing with the dimensions shown in Fig. 1. The total number of elementary volumes used to model the whole system is $N = 10 \times 10^3$; the magnet and the SC are discretized respectively with $n = 75$ and $m = 9925$ elements.

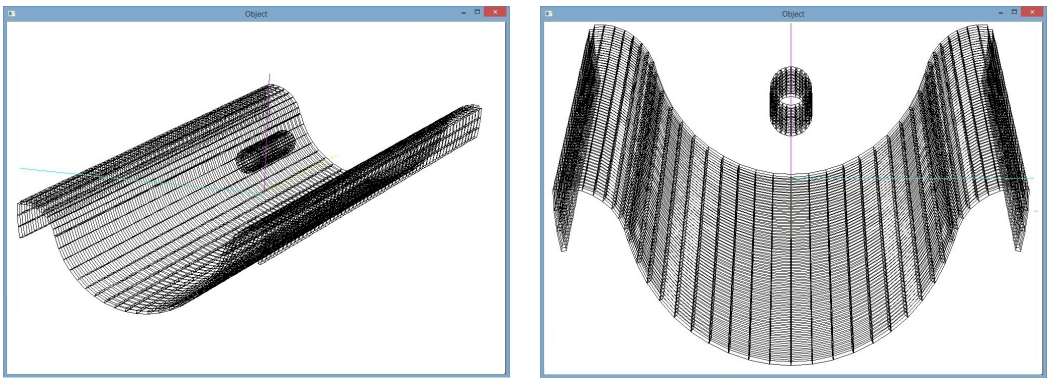

Figure 6. The mesh used by the numerical code to simulate the whole system.

Although the code is able to deal with all the 6 DOF, in Section 4 some constraints reducing the number of DOF have been introduced in order to allow the comparison with the results described in [18]. In Section 5 the system has been simulated considering only 3 DOF (preventing rotations of the PM) in order to verify the consistency of the results.

4. STATIC CALCULATIONS

4.1. Stable Levitation Position

The lift force was calculated in two different positions of the magnet. The first one is the center of the reference frame (see Fig. 1) at $z = 0.0$ mm and the second one is on a height at which the lift force can compensate the weight of the magnet ($z = 2.3$ mm). The results are displayed in Fig. 7.

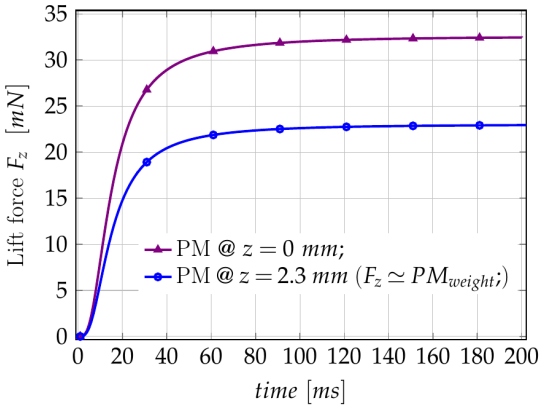

Figure 7. Lift force versus time for $z = 0.0$ mm and $z = 2.3$ mm.

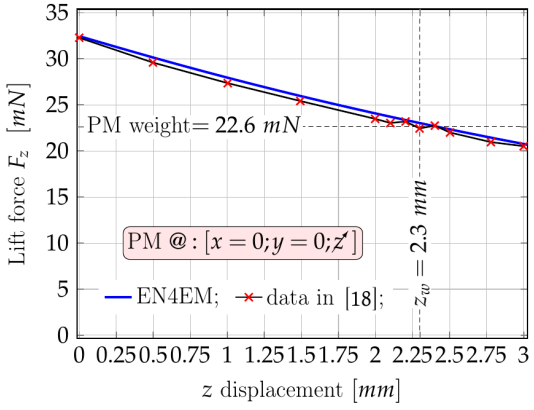

Figure 8. Lift force versus z displacement for $x = 0.0$ mm and $y = 0.0$ mm.

The transient behavior of the lift force is due to the profile of the magnetization current, used to model the permanent magnet (see Fig. 3). At the time of about 200 ms the magnetization current has reached its rated value and the lift force assumes the values of about 32.5 mN and 22.6 mN, when the PM is positioned respectively at $z = 0.0$ mm and $z = 2.3$ mm.

In order to get the understanding how the lift force varies with respect to the magnet position on the z-axis we performed a simulation forcing the magnet to slowly move on this axis. The evolution of the lift force after the magnetization current have reached its rated value, was calculated. The results, displayed in Fig. 8, are compared with the ones from [18], showing a very good agreement.

4.2. Passive Stable Position

From the previous equilibrium position, the magnet has been forced to move on the y direction in order to determine the value and direction of the lift and lateral forces (F_z and F_y). Both results are presented in Fig. 9. As can be seen, they are really close to the ones reported in [18]. Furthermore, the stabilizing characteristic of the lateral force F_y is noteworthy. As the displacement increases along the positive direction of the y-axis, the force F_y negatively increases, tending to bring the magnet in its original position.

4.3. Border Effects

We also perform some simulations to see the behavior when the magnet reaches the end of stroke. The results differ from the ones reported in [18] probably because of the different shapes of the SC edge. As shown in Fig. 1, the two SC edges positioned at $x = \pm 150$ mm and simulated by the FEM code are somehow smoothed, while the model simulated by the EN4EM code has sharp edges. This choice was suggested by the fact that in the standard operating conditions, the permanent magnet is positioned in the area near the center of the U-shaped superconducting surface, far from both ends. Then, in order to avoid the increasing complexity of the numerical model, the simulated system is simplified in this paper, cutting the edges at the ends of the U-shaped bed. The trend of the lift force is shown in Fig. 10(a), while Fig. 10(b) shows the axial force F_x. It is interesting to note that when reaching the stroke end, there is also a pitch torque, as shown in Fig. 10(c).

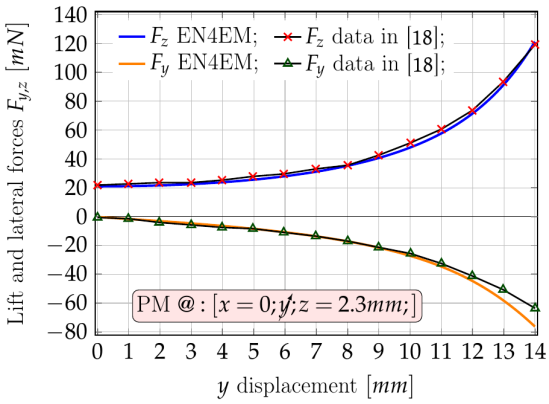

Figure 9. Lift force F_z and lateral force F_y versus y displacement for $x = 0.0\,\text{mm}$ and $z = 2.3\,\text{mm}$.

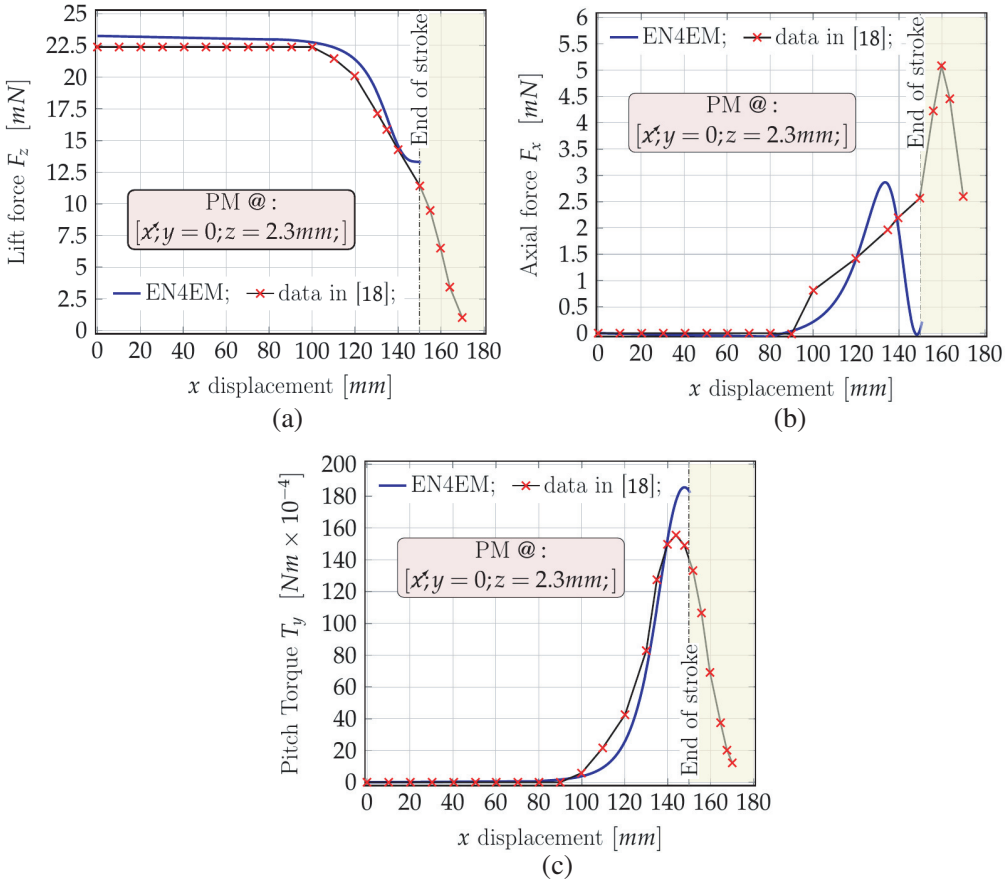

Figure 10. The effect of the SC border: forces and torque as a function of x displacement, for $y = 0.0\,\text{mm}$ and $z = 2.3\,\text{mm}$. (a) Lift force F_z. (b) Axial force F_x. (c) Pitch torque T_y.

The comparison of the results of the present study with those reported in [18] shows that for all the compared quantities described in Figs. 10(a) and 10(b) the maximum percentage error is always below $5 \div 8\%$. On the contrary, when the permanent magnet reaches the end of the U-shaped SC, an unsatisfactory agreement affects the comparison of results of the axial force F_x (see Fig. 10(b)). In this case, the errors exceed 45%. Anyhow, it is noteworthy that when the magnet is positioned in the standard operating range along the axis of the U-shaped SC ($\pm 90\,\text{mm}$), the results of the axial force F_x obtained by the EN4EM code are in good agreement with the ones in [18].

5. DYNAMIC CALCULATIONS

We also perform two simulations of the system with the magnet free to move with 3 DOF obtained by preventing the rotations of the PM. Fig. 11(a) shows the simulation results of the dynamic behavior of the system under the following conditions: in the time range $[0 \div 0.2]$ s the magnet (PM) has been kept blocked at $x = 0.0$ mm, $y = 0.0$ mm and $z = 0.0$ mm in order to reach the end of the transient phase of the magnetization current. In this condition, the magnet is fixed in the origin of the reference frame, and the force acting on the PM reaches its maximum value of about 32.5 mN. At the time 0.2 s, the constraint has been removed, and the magnet, whose weight in term of gravity force is about 22.6 mN, has been left free to move. Since the total force F_z is the vectorial sum of the lift force and the weight of the magnet, at the time 0.2^+ s, the PM feels a net force of about 10 mN. As a consequence, the magnet starts to move on the z-axis increasing the displacement of its center of mass until the lift force becomes zero. At this point, the gravity force tends to reduce the z-displacement, and when the lift force equals the gravity force, it is about 2.3 mm. Anyhow, disregarding an eventual damping, the permanent magnet moves on the z-axis with an oscillating behavior.

Another simulation has been performed with the center of gravity of the magnet starting in $x = 0.0$ mm and $z = 0.0$ mm with a y displacement of 5.0 mm. The total force F_z (lift+PM weight) and the lateral force F_y waveforms as function of time are shown in Fig. 11(b). Also in this case, the magnet moves with an oscillating behavior.

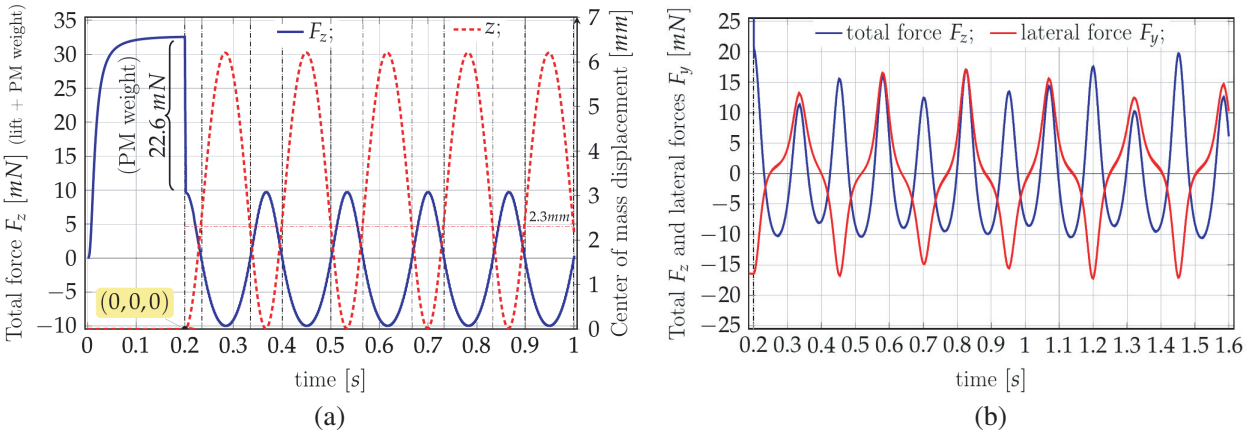

Figure 11. Dynamic behavior of the device. (a) The total force F_z (lift+PM weight) and Center of mass displacement in the z axis. (b) The total force (F_z) and lateral force (F_y) dynamics starting from $x = 0.0$ mm, $y = 5.0$ mm and $z = 0.0$ mm.

Anyhow, such forces tend to bring the permanent magnet in its equilibrium position.

6. CONCLUSION

The analysis of a non-Hysteretic Superconductive Passive Magnetic Linear Bearing has been presented. The simulations have been performed by the use of a numerical code based on a 3D integral formulation, previously developed at the University of Pisa for research purposes, and capable to simulate coupled electro/mechanical problems with six degree of freedom (6 DOF). The static results have been compared with the ones described in a previous paper, showing a quite good agreement. Furthermore, some preliminary dynamic simulations have been described which are consistent with the expected behavior of the device. The ongoing work is aimed at developing a suitable prototype, necessary to validate the numerical model by means of experimental measurements.

ACKNOWLEDGMENT

The authors would like to thank NVIDIA's Academic Research Team for their equipment donation of two NVIDIA Tesla K20c GPUs that have been extensively exploited for the simulation activity.

REFERENCES

1. ESA, "European non-dependence on critical space technologies: Actions for 2009," Report, 2009.
2. Van Den Dool, T. C., F. Kamphues, W. L. M. Gielesen, and B. C. Braam, "Magnetic bearing based cryo-mechanisms for future IR missions," *astro2010: The Astronomy and Astrophysics Decadal Survey*, Vol. 2010, No. 0, 33, 2009.
3. Iizuka, T. and H. Fujita, "Precise positioning of a micro conveyor based on superconducting magnetic levitation," *Proc. of Int. Symp. on Micromechatronics and Human Science*, 131–135, 1997.
4. Di Dio, V. and M. Montana, "State of art of tubular linear induction motor," *Proc. of the Mediterranean Electrotechnical Conference — MELECON*, Vol. 1, 285–288, 1996.
5. Di Dio, V., G. Cipriani, M. Corpora, D. Curto, and M. Trapanese, "A Ferrite Tubular Linear Motor (FTLM): Analysis and design," *2015 IEEE Magnetics Conference (INTERMAG)*, 1–1, Beijing, 2015.
6. Di Dio, V., G. Cipriani, R. Miceli, and R. Rizzo, "Design criteria of tubular linear induction motors and generators: A prototype realization and its characterization," *Leonardo Electronic Journal of Practices and Technologies*, Vol. 12, Issue 23, 19–40, Jul. 2013.
7. Theiler, G., T. Gradt, and P. Klein, "Friction and wear of PTFE composites at cryogenic temperatures," *Tribol. Int.*, Vol. 35, 449–458, 2002.
8. Fleischer, N., M. Genut, L. Rapoport, and R. Tenne, "New nanotechnology solid lubricants for superior dry lubrication," *Proceedings of the 10th European Space Mechanisms and Tribology Symposium*, 65–66, 2003.
9. Choi, Y. M. and D. G. Gweon, "A high-precision dual-servo stage using Halbach linear active magnetic bearings," *IEEE/ASME Trans. Mechatronics*, No. 99, 1–7, 2011.
10. Hol, S. A. J., E. Lomonova, and A. J. A. Vandenput, "Design of a magnetic gravity compensation system," *Precis. Eng.*, Vol. 30, 265–273, 2006.
11. Arkadiev, V., "A floating magnet," *Nature*, Vol. 160, No. 4062, 330–330, Sep. 1947.
12. Hull, J. R., "Superconducting bearings," *Superc. Sci. Technol.*, Vol. 13, No. 2, 1–15, Jul. 2000.
13. Perez-Diaz, J. L., I. Valiente-Blanco, E. Diez-Jimenez, and J. Sanchez-Garcia-Casarrubios, "Superconducting non-contact device for precision positioning," *IEEE/ASME Trans. on Mechatronics*, Vol. 19, No. 2, 2014.
14. Diez-Jimenez, E. and J. L. Perez-Diaz, "Foundations of meissner superconductor magnet mechanisms engineering," *Superconductivity — Theory and Applications*, 153–172, 2011.
15. Iizuka, T., N. Sakai, and H. Fujita, "Position feedback control using magneto impedance sensors on conveyor with superconducting magnetic levitation," *Sensors Actuators A Phys.*, Vol. 150, No. 1, 110–115, Mar. 2009.
16. Serrano-Tellez, J., F. Romera-Juarez, D. Gonzlez-de-Mara, M. Lamensans, H. Argelaguet-Vilaseca, J.-L. Prez-Daz, J. Snchez-Casarrubios, E. Diez-Jimenez, and I. Valiente-Blanco, "Experience on a cryogenic linear mechanism based on superconducting levitation," *Conf. on Modern Technologies in Space and Ground-Based Telescopes and Instrumentation*, 1–9, 2012.
17. Prez-Daz, J., "Non-contact linear slider for cryogenic environment," *Mach. Theory*, Vol. 49, 308–314, 2012.
18. Diez-Jimenez, E., I. Valiente-Blanco, V. Castro-Fernandez, and J. L. Perez-Diaz, "Design and analysis of a non-hysteretic passive magnetic linear bearing for cryogenic environments," *Proc. of the Inst. of Mech. Eng., Part J: Jour. of Eng. Tribology*, Mar. 25, 2014.

19. Davat, B., Z. Ren, and M. Lajoie-Mazenc, "The movement in field modeling," *IEEE Transactions on Magnetics*, Vol. 21, No. 6, 2296–2298, Nov. 1985.
20. Bossavit, A., *Computational Electromagnetism: Variational Formulations, Complementarity, Edge Elements*, Academic Press, 1998.
21. Rodger, D., H. C. Lai, and P. J. Leonard, "Coupled elements for problems involving movement," *IEEE Transactions on Magnetics*, Vol. 26, No. 2, 548–550, Mar. 1990.
22. Albanese, R. and G. Rubinacci, "Integral formulation for 3D eddy-current computation using edge elements," *IEEE Proceedings A (Physical Science, Measurement and Instrumentation, Management and Education, Reviews)*, Vol. 135, No. 7, 457–462, 1988.
23. Musolino, A., R. Rizzo, E. Tripodi, and M. Toni, "Modeling of electromechanical devices by GPU-accelerated integral formulation," *International Journal of Numerical Modelling: Electronic Networks, Devices and Fields*, Vol. 26, No. 4, 376–396, Jul./Aug. 2013.
24. Esposito, N., A. Musolino, and M. Raugi, "Modelling of three-dimensional nonlinear eddy current problems with conductors in motion by an integral formulation," *IEEE Transactions on Magnetics*, Vol. 32, No. 3, 764–767, 1996.
25. Musolino, A., R. Rizzo, and E. Tripodi, "Tubular linear induction machine as a fast actuator: Analysis and design criteria," *Progress In Electromagnetics Research*, Vol. 132, 603–619, 2012.
26. Musolino, A., R. Rizzo, M. Toni, and E. Tripodi, "Acceleration of numerical formulations by using graphic processing units and its application in electromagnetic launcher modeling," *IEEE Transactions on Plasma Science*, Vol. 41, No. 5, 1104–1111, 2013.
27. Tripodi, E., A. Musolino, R. Rizzo, and M. Raugi, "A new predictor-corrector approach for the numerical integration of coupled electromechanical equations," *International Journal for Numerical Methods in Engineering*, Vol. 105, No. 4, 261–285, 2016.
28. Barmada, S., A. Musolino, M. Raugi, and R. Rizzo, "Numerical simulation of a complete generator-rail launch system," *IEEE Transactions on Magnetics*, Vol. 41, 369–374, 2005.